
# A High Temperature, Ultra High Vacuum Facility for Heavy Ion Simulation of Neutron Radiation Damage to Potential Reactor Materials

H.V. Smith, Jr. and R.G. Lott

January 1977

UWFDM-189

FUSION TECHNOLOGY INSTITUTE

UNIVERSITY OF WISCONSIN

MADISON WISCONSIN

# A High Temperature, Ultra High Vacuum Facility for Heavy Ion Simulation of Neutron Radiation Damage to Potential Reactor Materials

H.V. Smith, Jr. and R.G. Lott

Fusion Technology Institute
University of Wisconsin
1500 Engineering Drive
Madison, WI 53706

http://fti.neep.wisc.edu

January 1977

UWFDM-189

# A High Temperature, Ultra High Vacuum Facility for Heavy Ion Simulation of Neutron Radiation Damage to Potential Reactor Materials*

H. Vernon Smith, Jr.† and R. G. Lott, Department of Nuclear Engineering
University of Wisconsin, Madison, Wisconsin 53706 USA

## Abstract

The University of Wisconsin-Madison facility for simulating neutron damage to potential reactor materials is described. Heavy metal ions from a tandem accelerator bombard metal specimens heated as high as 1000°C at pressures below $10^{-8}$ Torr. Special features of the facility include a radiation heater assembly which allows integration of the beam current, an ultra high vacuum environment which is characterized by partial pressure analysis, use of 15-20 MeV heavy metal ions to induce the damage in the specimens, and direct measurement of the beam composition. This facility is suitable for studying radiation effects in the refractory metals as well as other potential reactor materials.

## 1. Introduction

Void swelling is an important problem to overcome for successful commercial operation of the liquid metal fast breeder reactor (LMFBR) and proposed magnetically confined and inertial (e.g., laser-driven) fusion reactors. Originally, volume increase of the graphite moderators in fission reactors was predicted [1,2]. In 1966, Cawthorne and Fulton[3]) reported that fast neutron irradiated stainless steel exhibits void swelling. Since that time much work has been done to assess the dimensional (volume increase) and structural (radiation induced creep, etc.) stability of materials in a neutron environment.

*Work supported in part by the Division of Physical Research, United States Energy Research and Development Administration.
†Mailing address: Department of Physics, 1150 University Avenue, University of Wisconsin, Madison, Wisconsin 53706 USA.

Components in and near the core of LMFBR's and the first wall of fusion reactors will be subjected to total neutron fluences of $\gtrsim 10^{23}$ neutrons/cm$^2$ over the reactor lifetime. Since existing neutron sources have strengths $<10^{15}$ neutrons/cm$^2$/sec, the times required to duplicate the damage level attained over the reactor lifetime are $\gtrsim 10^8$ sec (3 yr). The long times required for neutron experiments on proposed reactor materials are unsatisfactory from both experimental and program development points of view. The heavy ion simulation technique[4,5]) overcomes this difficulty and offers some additional advantages (e.g., cost reduction, controlled experimental conditions) over in-reactor experiments.

The basis of the heavy ion simulation technique is illustrated in fig. 1. Energetic heavy ions, e.g. 20 MeV Ni, impinge normal to the specimen surface, are slowed by electronic and nuclear interactions with the specimen's lattice atoms, and come to rest several μm from the specimen's surface. The energy given up to electronic excitation is lost to the technique. However, those lattice atoms which receive an energy greater than the displacement energy, 24 eV for nickel, by nuclear collisions with either an incident ion or a recoiling lattice atom are displaced thus forming vacancy-interstitial

pairs as in neutron irradiation. The fate of the individual vacancies and interstitials determines the material's response to the radiation environment. The energetic heavy ions have $10^5$ - $10^6$ larger displacement rates than reactor neutrons. The resulting higher damage rate allows a given damage state to be attained more quickly by ion bombardment than neutron irradiation. The specimens are examined in a ~1500 Å thick region ~1 μm from the surface by transmission electron microscopy. A more complete discussion of the heavy ion simulation technique, including its advantages and disadvantages, is contained in a recent review article[6]) and the references contained therein.

The refractory metals and their alloys are under consideration for use in and near the first wall of fusion reactors[6]). Ion simulation studies of these materials are complicated by the fact that they are easily contaminated by interstitial impurities if stringent vacuum requirements are not met[7]). Standards for heavy ion simulation of neutron damage have been detailed by the E10.08 subcommittee of the American Society of Testing Materials (ASTM) in ref. 8. The apparatus described below, used primarily for studying void swelling in the refractory metals, is designed to meet these requirements. An earlier description of this system is contained in ref. 9.

## 2. Experimental Apparatus

A schematic drawing of the experimental system is shown in fig. 2. The heavy ion source, accelerator, and sample chamber used in the heavy ion simulation experiments are described below.

### 2.1. ION SOURCE

The SPIGS (Sputter Penning Ion Gauge Source) described in ref. 10 has provided the negative metal ions for the irradiations performed to date. In SPIGS

negative metal ions are probably formed by Cs-assisted sputtering of the cathodes. SPIGS gives several μA beams of $Cu^-$ and $Ni^-$ but disappointingly low currents (≲200 nA) of the refractory metals (table 2 of ref. 10). The $Cu^-$ beam has been used for most of the heavy ion irradiations. Some Ni "self-ion" irradiated specimens have been prepared.

The low electron affinity of the refractory metals is probably responsible for their low output from SPIGS[11]). A newly constructed version of SPIGS[11]) which is based on the ANIS source[12]) will be used for "self-ion" irradiations of refractory metal specimens. ANIS is similar to SPIGS but incorporates a third sputter cathode which is placed directly across from the extraction aperture (fig. 5 of ref. 11). Outputs of 1 μA for $Al^-$ and 3μA for $Ta^-$ have been reported for ANIS[12]) and 0.8 μA of $V^-$ and 1 μA of $Nb^-$ have been obtained in tests by one of us (HVS). A $He^-$ source is available to implant He into the specimens, either prior to or in several stages alternating with irradiation.

## 2.2. ACCELERATOR

The University of Wisconsin-Madison tandem Van de Graaff accelerator (HVEC model EN) accelerates the heavy metal ion beams used to irradiate the specimens. Nitrogen stripper gas is used in place of thin carbon foils because foils have short lifetimes under heavy ion bombardment[13]).

The mass-energy product, $mE/q^2$ (where m, E, and q are the ion beam mass, energy, and charge respectively), of the accelerator analyzing magnet is 30 MeV-AMU, too low to bend the heavy metal ion beams into the established target rooms. Therefore, the specimen chamber is located near the tandem axis as shown in fig. 2. A 1/8° bend combined with a 4 m drift to a 3 mm dia. aperture before the specimen provides sufficient magnetic analysis to prevent unwanted bombardment of the samples by neutrals and low Z ions from the accelerator (see section 2.3c below).

## 2.3. SAMPLE CHAMBER

The specimens to be irradiated must be heated in a vacuum environment to prevent pickup and subsequent diffusion of impurities into the damage region (~1 μm from the surface). For the same reason the heavy ion beam must be free of contaminants. The ion beam must be well characterized to properly assess the damage state attained in the irradiation. Below the method of heating the specimens, the apparatus used to provide the UHV vacuum environment, and the method of determining the beam energy, composition, fluence†, and intensity profile are described.

### 2.3a. FURNACE

For studying void formation in the refractory metals the heater must be able to attain temperatures up to 1000°C or more since voids are formed in metals at temperatures between 0.3 and 0.6 of the absolute melting point[6]). The materials used in construction of the heater must maintain UHV vacuum properties at their operating temperature. In addition, the specimen beam current should be integrated to properly determine the heavy ion fluence. In order to meet these requirements, the specimens are heated with a thermal radiation heater (fig. 3) patterned after that of Rendall[14]).

Power is transferred to the Ta sample holder by radiation from a 4 cm dia., 10 cm long cylindrical heater. The heater and surrounding 15 turn spirally wound heat shield[15]) are constructed from 0.025 mm Ta sheet. The heater and heat shield are suspended from stainless steel collars. The beam is transmitted through 1.0 cm concentric holes in the heater and heat shield for either sample irradiation or beam analysis. The cylindrical heater is heated by an AC current: 200 A are required for the heater to attain 1200°C which results in a sample

---

†Number of beam particles per unit area.

temperature near 1000°C. This design reliably operates at sample temperatures above 400°C for more than 1500 hours before heater replacement is required. This heater has been used to anneal V samples *in situ* at 1100°C and to irradiate Mo samples at 1000°C.

The samples are held by the Ta sample holder (fig. 4) which is suspended along the axis of the cylindrical heater shown in fig. 3. An adjustable bellows seal allows motion of the sample holder along the heater axis. This feature is used to irradiate up to eight different specimens without breaking the vacuum. The eight specimen positions are separated by three 4.8 mm dia. holes to transmit the beam for further analysis (see section 2.3c below). The specimens are in disc form, 3 mm dia. x~0.1 mm thick, to facilitate post-irradiation examination in an electron microscope. The specimens are irradiated in descending temperature steps to reduce post-irradiation annealing effects.

Chromel-alumel thermocouples are used to measure the temperature of each specimen. When the sample holder is centered in the furnace, the total temperature difference indicated by the thermocouples is 18°C for temperatures near 800°C. Osgood *et al.*[16]) also report a very uniform temperature distribution along a similarly constructed radiation heater. No control circuit is necessary to maintain temperatures to within ±5°C over long time periods (~10 hours). The 1/2 watt power input to the samples from the beam causes <3°C rise in sample temperatures near 700°C.

### 2.3.b VACUUM SYSTEM

The accelerator beam line pressure near the 90° analyzing magnet is near $5 \times 10^{-6}$ Torr.† Pressures below $1 \times 10^{-8}$ Torr are required for the sample environment[8]). The differential pumping arrangement shown in fig. 5 is used

†Unless otherwise noted, all pressures reported in this paper are direct readings from an ionization gauge *uncorrected* for the gauge sensitivity to the constituent gases.

to meet this requirement. The first of three pumping stages employs a 200 liter/sec diffusion pump equipped with a liquid nitrogen cold trap to attain pressures near $2 \times 10^{-6}$ Torr. An anti-creep liquid nitrogen cold trap, protected from stray beam particles by a Ta aperture, separates the first pumping stage from the intermediate pumping stage. The conductance of the aperture-cold trap combination is 2 liters/sec for nitrogen.

An orbitron pump[17]) having a puming speed of 300 liters/sec for air is used to attain a pressure of $1 \times 10^{-7}$ Torr in the intermediate pumping stage. With the exception of the isolation valve between the first and intermediate pumping stages, all vacuum seals in the intermediate pumping stage are made with aluminum gaskets. Ungreased Viton "O"-rings are used in the isolation valve. A pumping impedance comprised of a stack of fifteen 6.5 mm dia. Ta apertures providing a total conductance of 0.25 liters/sec for nitrogen separates the intermediate stage from the sample chamber stage.

The sample chamber stage is pumped by a combination titanium sublimitation-ion pump† having a pumping speed of 600 liters/sec for air. The sample chamber stage is constructed of stainless steel. All vacuum seals in the sample chamber stage are made with either aluminum or copper metal gaskets. An all-metal valve isolates the intermediate and sample chamber stages. After bake-out, the base pressure of the isolated sample chamber stage is $5 \times 10^{-10}$ Torr as indicated by the Bayard-Alpert gauge.†† When the metal specimens are heated to 1000°C, the pressure in the sample chamber stage will remain below $1 \times 10^{-8}$ Torr. The walls of the furnace region are externally water cooled.

---

†Getter-Ion Pump Model No. OSP7-89 manufactured by National Electrostatics Corporation, Middleton, Wisconsin, USA.

††WL-5966 manufactured by Westinghouse Electric Corporation, Elmira, New York, USA.

A residual gas analyzer† (RGA) is used to monitor the partial pressure composition of the sample chamber environment. The RGA also serves as an instantly available He leak chaser. The partial pressure composition of the sample environment during the in situ anneal and subsequent irradiation of a series of vanadium specimens is shown in fig. 6. The 1050°C scan was taken during the one hour anneal of the specimens at a total pressure of $5 \times 10^{-8}$ Torr (the sample chamber was isolated). The 650°C scan was taken during the irradiation of one of these specimens at $7 \times 10^{-9}$ Torr. It is observed that under irradiation conditions opening the beam line valves does not significantly alter the partial pressure composition of the sample chamber stage. The results displayed in fig. 6 have been adjusted for the sensitivity of the RGA for the various gaseous species[18]) and then normalized to the Bayard-Alpert gauge reading. Correcting the Bayard-Alpert gauge pressure indication for the gauge sensitivity to each of the constitutent gases[19]) gives total pressures of $6 \times 10^{-8}$ Torr at 1050°C and $1 \times 10^{-8}$ Torr at 650°C.

For sample temperatures under 1000°C, $H_2$ is the major constituent of the residual gas; above 1000°C, $H_2$ and CO predominate. The hydrogen, water vapor, and carbon monoxide probably evolve from the stainless steel used in the construction of the vacuum jacket and portions of the heater assembly[20]). The pressure of the system might be lowered if those parts of the heater which operate at elevated temperature (e.g., the collars) were constructed from a refractory metal rather than stainless steel. The hydrocarbons methane and ethylene as well as the carbon dioxide probably come from the stainless steel but some of the $H_2$ and $CH_4$ may be due to displacement of these species from the Ti layer on the walls of the sublimination-ion pump[21]).

---

†VGA-100 Quadrupole Gas Analyzer Model No. 978-1000, manufactured by Varian Associates, Palo Alto, California, USA.

The $CH_4$ and $C_2H_4$ compositions are distinguished from $O_2$ and CO respectively by careful consideration of the cracking patterns[18]) which give peaks at masses other than 16 and 28 respectively. The $N_2$ and $O_2$ partial pressures are less than $5 \times 10^{-11}$ Torr.

2.3c. ION BEAM ANALYSIS

The energy, composition, intensity, and uniformity of the ion beam striking the samples must be measured so that the damage state of the specimens may be determined. A direct measure of the beam composition is particularly important since the sample chamber is located only 1/8° off the tandem axis. Nitrogen ions can be formed in the $N_2$ gas stripper canal in the accelerator terminal and transmitted to the sample chamber along with the heavy metal ion beam, resulting in accidental contamination of the specimens.

The beam energy, E, is determined by the accelerator terminal voltage, V, and the ion beam charge state, q, since

$$E = (q + 1)V \qquad (1).$$

A digital voltmeter, calibrated by magnetic analysis of a beam with known energy and charge state, is used to measure the terminal voltage. The composition of the heavy metal ion beam is determined by recording in a solid state detector (fig. 7) the energy of the beam particles elastically scattered through 90° by a thin gold foil[22]). A typical spectrum obtained for a Cu beam is shown in fig. 8a. The positions of the $Cu^{0+}$ to $Cu^{6+}$ charge states along with the expected locations of the $N^+$ and $N_2^+$ peaks are marked in the figure. Corrections have been made for the pulse height defect[23]) in determining the peak positions. Adjusting the spectrum in fig. 8a for the mass and energy dependence of the laboratory Rutherford cross section yields the beam particle composition shown in fig. 8b. The beam is almost entirely composed of $Cu^{4+}$ (95.1%). Small

amounts of $Cu^{1+}$ (0.06%) and $Cu^{2+}$ (4.8%) are also present. Possible nitrogen components in the beam are so weak (<0.1% each) that they are undetected.

The fluence of beam particles striking the samples is determined by the mask aperture area, the time integrated beam current, and the charge state distribution of the beam. The sample heater, heat shield, and sample holder are connected together to form a Faraday cup (fig. 3) and positively biased to suppress secondary electrons. The gold target (fig. 7) may be removed from the beam to allow a check of the sample current with the Faraday cup 40 cm downstream from the samples. These two measurements agree to within 2%.

The damage state attained in the region of the specimen examined in the transmission electron microscope is calculated using the E-DEP-1 code of Manning and Mueller[24]). The E-DEP-1 code calculates the electronic and nuclear energy loss to determine the number of displaced atoms as a function of depth. Only the portion lost by nuclear collisions results in displaced lattice atoms. The result of such a calculation for 20 MeV Ni on Ni is shown in fig. 1. Note that the Ni ions are deposited ~2.5 μm from the sample surface which makes examination of the damage zone $\geq$1 μm from both the stopped ions and the sample surface possible. If low energy ($\lesssim$3 MeV) ions are used the damage region must be examined much closer to either the specimen surface or the stopped ions since then the ion range is only ~1 μm.

The major uncertainty in determining the damage state of the specimens is the nonuniformity of the ion beam intensity$_{\Lambda}^{\text{profile}}$ - only $10^{-4}$ of the irradiated area is usually examined in the electron microscope. Measurements with the adjustable slits located 1.9 m in front of the samples (fig. 5) show that the beam$_{\Lambda}^{\text{profile}}$ is uniform to within $\pm$20% at the slits. This is a good indication of the beam uniformity at the samples since the adjustable slits are located 5.4 m from the last focusing device. Rastering the beam to obtain uniformity

is avoided because of possible deleterious effects on the void swelling measurements[25]).

Typical sample beam currents are 20 particle nA with fluctuations less than 25%. The resulting displacement rates, $5 \times 10^{-4}$ dpa/sec ~1 μm from the specimen surface and $5 \times 10^{-3}$ dpa/sec at the peak of the damage curve, are lower than those (up to $10^{-1}$ dpa/sec) obtained elsewhere[4,5]). However, the lower beam currents result in negligible beam heating of the specimens.

## 3. Results

Specimens of aluminum[26]), molybdenum[27]), nickel[28]), vanadium[29]), and vanadium-nitrogen alloy[26]) have been irradiated using this facility. The damage region is examined using transmission electron microscopy as described in ref. 8. First a ~ 1 μm surface layer is chemically removed to eliminate possible surface effects. The thickness removed is determined to within ± 0.1 μm by optical interference microscopy. The specimens are then back thinned to perforation to produce a thin foil (~1500 Å) in the plane perpendicular to the beam. The foil thickness is determined to within ± 15% in the electron microscope by the stereo pair technique.

An electron micrograph of a molybdenum specimen irradiated at 1000°C and prepared as described above is shown in fig. 9. The damage level in the region of analysis is 1.3 ±0.3 dpa. The error is due primarily to the beam nonuniformity (± 20%) with additional error (± 6%) due to the uncertainty in the exact location of the analysis region along the damage curve (fig. 1 ). The average void density is $6 \times 10^{14}/cm^3$ (± 25% error due to the ± 15% uncertainty in the foil thickness and ± 5%, added twice, due to the uncertainty in the electron microscope calibration). The avg. void diameter is 250 Å (± 5% error due to the uncertainty in the magnification of the electron microscope). The resulting volume increase in the analysis region is 0.76 ± 0.15%. As discussed in ref. 6, correlation of heavy ion induced damage with neutron induced damage is required before the behavior of a material in a neutron environment may be predicted from ion simulation data.

## 4. Conclusions

The University of Wisconsin-Madison facility for simulating neutron damage is suitable for studying void swelling in refractory metals as well as in other materials with less stringent requirements. This facility has the special features of an ultra high vacuum specimen environment, partial pressure analysis of the specimen environment, use of a 15-20 MeV heavy metal ions to induce the damage, thorough analysis of the heavy metal ion beam, the capability to anneal specimens in situ at temperatures of 1100°C and pressures below $5 \times 10^{-8}$ Torr, and a capacity of eight specimens. Limitations of the present facility are low average dpa rates ($\lesssim 5 \times 10^{-4}$ dpa/sec ~ 1 μm from the specimen surface, $\lesssim 5 \times 10^{-3}$ dpa/sec at the peak of the damage curve), small specimen area (0.1 $cm^2$), and possible post-irradiation annealing effects in all but the last sample irradiated.

The authors gratefully acknowledge the support and encouragement of G. L. Kulcinski and H. T. Richards and the use of the tandem accelerator and its facilities by the University of Wisconsin nuclear physics group. R. C. Walsh machined most of the parts for the sample chamber and E. K. Opperman, W. J. Weber, and J. B. Whitley assisted in its construction. K. Y. Liou did the microscopy of the molybdenum specimen.

## References


1) F. Seitz, Phys. Today 5 no. 6 (1952) 6.

2) R. G. Hewlett and O. E. Andersson, Jr., The New World, 1939/1946 (The Pennsylvania State University Press, 1962) p. 630.

3) C. Cawthorne and E. J. Fulton, The Nature of Small Defect Clusters, ed. M. J. Mankin, UKAEA Report AERE-R5269 (1966) p. 446; Nature 216 (1967) 575.

4) S. F. Pugh, M. H. Loretto,and D. I. R. Norris (editors), Voids Formed by Irradiation of Reactor Materials, Reading, U. K., March 24-25, 1971, British Nuclear Energy Society.

5) J. W. Corbett and L. C. Ianniello (editors), Radiation-Induced Voids in Metals, Albany, N.Y., U.S.A., June 9-11, 1971, AEC Symposium Series (CONF-710601).

6) F. L. Vook et al., Rev. Mod. Phys. 47 (Supplement No. 3) (1975) S1.

7) E. Fromm, J. Vac. Sci. Technol. 7(1970) S100.

8) "Proposed New Standard Recommended Practice for Neutron Radiation Damage Simulation by Charged-Particle Irradiation," E521-00 (Prepared under the jurisdiction of ASTM Committee E-10, Subcommittee E10.08). Revised December 12, 1974.

9) R. G. Lott and H. V. Smith, Jr., Proc. of Symp. on Experimental Methods for Charged-Particle Irradiations (CONF-750947) (Gatlinburg, 1975) p. 82.

10) H. V. Smith, Jr. and H. T. Richards, Nucl. Instr. and Meth. 125 (1975) 497.

11) H. V. Smith, Jr., I.E.E.E. Trans. Nucl. Sci. NS-23 (1976) 1118.

12) P. Tykesson, H. H. Andersen,and J. Heinemeier, I.E.E.E. Trans. Nucl. Sci. NS-23 (1976) 1104.

13) J. L. Yntema, I.E.E.E. Trans. Nucl. Sci. NS-23 (1976) 1133.

14) J. H. Rendall, J. Sci. Instr. 29 (1952) 248.

15) C. K. Crawford, J. Vac. Sci. Technol. 9 (1972) 23.

16) R. L. Osgood, C. Procik, A. H. Madjid, and W. F. Anderson, Jr., Rev. Sci. Instr. 45 (1974) 306.

17) R. A. Douglas, J. Zabritski and R. G. Herb, Rev. Sci. Instr. 36 (1965) 1.

18) Instruction Manual, Monitorr 700 Series Analyzers, IM-805, Aero Vac Division, High Voltage Engineering Corporation, Burlington, Massachusetts, USA.

19) F. Nakao, Vacuum 25 (1975) 431.

20) R. Calder and G. Lewin, Brit. J. Appl. Phys. 18 (1967) 1459.

21) A. K. Gupta and J. H. Leck, Vacuum 25 (1975) 362.

22) J. M. Freeman and B. W. Hooton, Nucl. Instr. and Meth. 111 (1973) 501.

23) S. B. Kaufman, E. P. Steinberg, B. D. Wilkins, J. Unik, A. J. Gorski, and M. J. Fluss, Nucl. Instr. and Meth. 115 (1974) 47.

24) I. Manning and G. P. Mueller, Comp. Phys. Comm. 7 (1974) 85.

25) J. A. Sprague, J. E. Westmoreland, F. A. Smidt, Jr., and P. R. Malmberg, Trans. Am. Nucl. Soc. 16 (1973) 70.

26) G. L. Kulcinski et al., University of Wisconsin - Madison Nuclear Engineering Department Progress Report No. COO-2206-7 (December, 1976).

27) H. V. Smith, Jr., G. L. Kulcinski, K. Y. Liou, and P. Wilkes, University of Wisconsin - Madison Nuclear Engineering Department Report UWFDM-177 (October, 1976).

28) J. B. Whitley, P. Wilkes,and G. L. Kulcinski, University of Wisconsin - Madison Nuclear Engineering Department Report UWFDM-159 (June, 1976).

29) W. J. Weber, G. L. Kulcinski, R. G. Lott, P. Wilkes, and H. V. Smith, Jr., Proc. Conf. on Radiation Effects and Tritium Technology for Fusion Reactors (CONF-750989) (Gatlinburg, 1975) p. I-130.

## FIGURE CAPTIONS

Figure 1. Depth distribution of the average number of displaced lattice atoms per lattice atom (in dpa) induced by 20 MeV Ni ions incident on nickel (solid curve). The Ni ions are incident from the left normal to the specimen surface. The depth distribution of the deposited Ni ions is also indicated on the figure (dashed curve). An advantage of using 15-20 MeV ions is that the damage region may be examined $\geq$ 1 μm from both the sample surface and the stopped ions.

Figure 2. Experimental layout of the heavy ion simulation facility at the University of Wisconsin-Madison. Heavy metal ions from the SPIGS source are injected into the tandem accelerator. The resulting energetic heavy ions, 20 MeV $Ni^{4+}$ in the example illustrated in the figure, bombard the metal specimens located in the sample chamber. The structural damage induced in the specimens by the heavy ions simulates that caused by reactor neutrons as discussed in ref. 6.

Figure 3. Specimen radiation heater assembly. The heater is a 0.025 mm thick Ta cylinder. The heat shield consists of 15 spirally wound turns of 0.025 mm Ta sheet. Detail of the sample holder assembly is shown in fig. 4.

Figure 4. Sample holder assembly. The eight specimens are in 3 mm dia. disc form to facilitate post-irradiation examination of the specimens in an electron microscope. When one of the three hole positions is selected through motion of a bellows assembly the beam is transported to the beam measurement devices shown in fig. 7.

Figure 5. Schematic of the sample chamber beam line. The three differential pumping stages which allow reduction of the pressure from $5 \times 10^{-6}$ Torr in the accelerator beam line to below $1 \times 10^{-8}$ Torr in the sample

chamber are shown. Other vacuum and beam analysis devices discussed in the text are indicated on the figure.

Figure 6. The partial pressure composition of the sample environment measured during the in situ anneal at 1050°C and 5 x $10^{-8}$ Torr and subsequent irradiation at 650°C and 7 x $10^{-9}$ Torr of a vanadium specimen.

Figure 7. Schematic of the heavy ion beam analysis devices. The mask aperture determines the area of the beam striking the specimens. The sample holder (fig. 4) may be moved to a hole position to allow measurement of the beam intensity profile with the beam profile monitor, the composition of the beam with the charge state device, or the intensity of the beam with the supressed Faraday cup.

Figure 8. a). A typical energy spectrum for a Cu beam at a terminal voltage of 3.75 MV. This spectrum was recorded in the solid state detector shown in fig. 7. The positions of the various Cu charge states and undetected $N^+$ and $N_2^+$ contaminants are indicated on the figure.

b). The beam particle composition determined from the spectrum shown in fig. 8a). Corrections for the mass and energy dependence of the laboratory Rutherford cross section have been made to obtain this distribution. The beam is almost entirely composed of $Cu^{4+}$ (95.1 %). Small amounts of $Cu^{1+}$ (0.06 %) and $Cu^{2+}$ (4.8 %) are detected. The other Cu charge states and possible nitrogen components are not detected. The upper limits assigned to these components are indicated on the figure.

Figure 9. Electron micrograph of a molybdenum specimen irradiated at 1000°C to a damage level of 1.3 dpa. The foil orientation is near {100}. The white cubical and octrahedral shaped features are voids - three dimensional aggregates of lattice vacancies. The volume increase of this specimen due to the presence of the voids is 0.8 %.

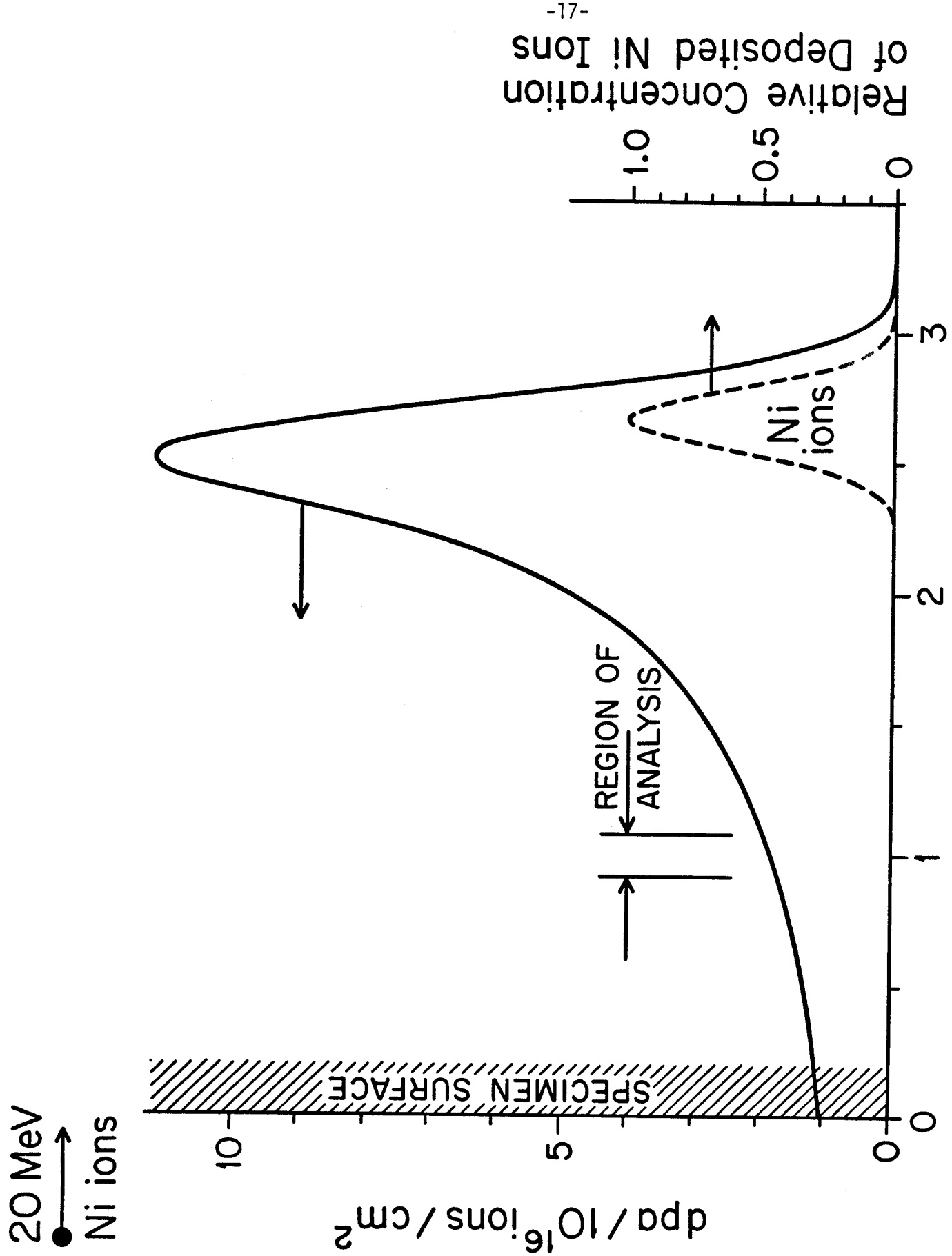
20 MeV
Ni ions
dpa / 10^16 ions / cm^2
10
5
0
SPECIMEN SURFACE
REGION OF ANALYSIS
Ni ions
0
1
2
3
Depth (μm)
Relative Concentration of Deposited Ni Ions
1.0
0.5
0

Figure 1

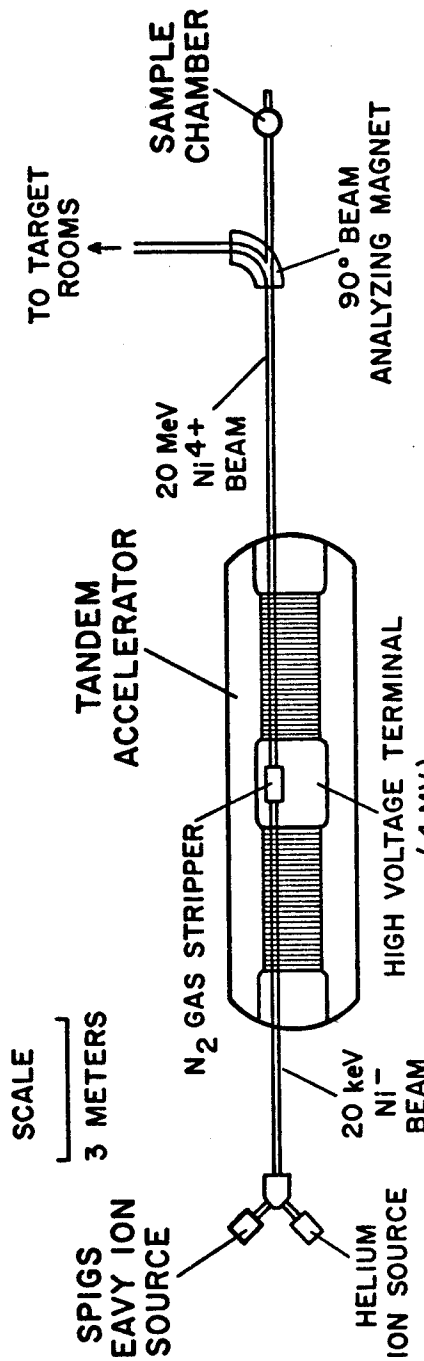
SAMPLE CHAMBER
TO TARGET ROOMS
90° BEAM ANALYZING MAGNET
20 MeV Ni4+ BEAM
TANDEM ACCELERATOR
N2 GAS STRIPPER
HIGH VOLTAGE TERMINAL (4 MV)
SCALE
3 METERS
20 keV Ni- BEAM
SPIGS HEAVY ION SOURCE
HELIUM ION SOURCE
UNIVERSITY OF WISCONSIN HEAVY ION SIMULATION FACILITY

Figure 2

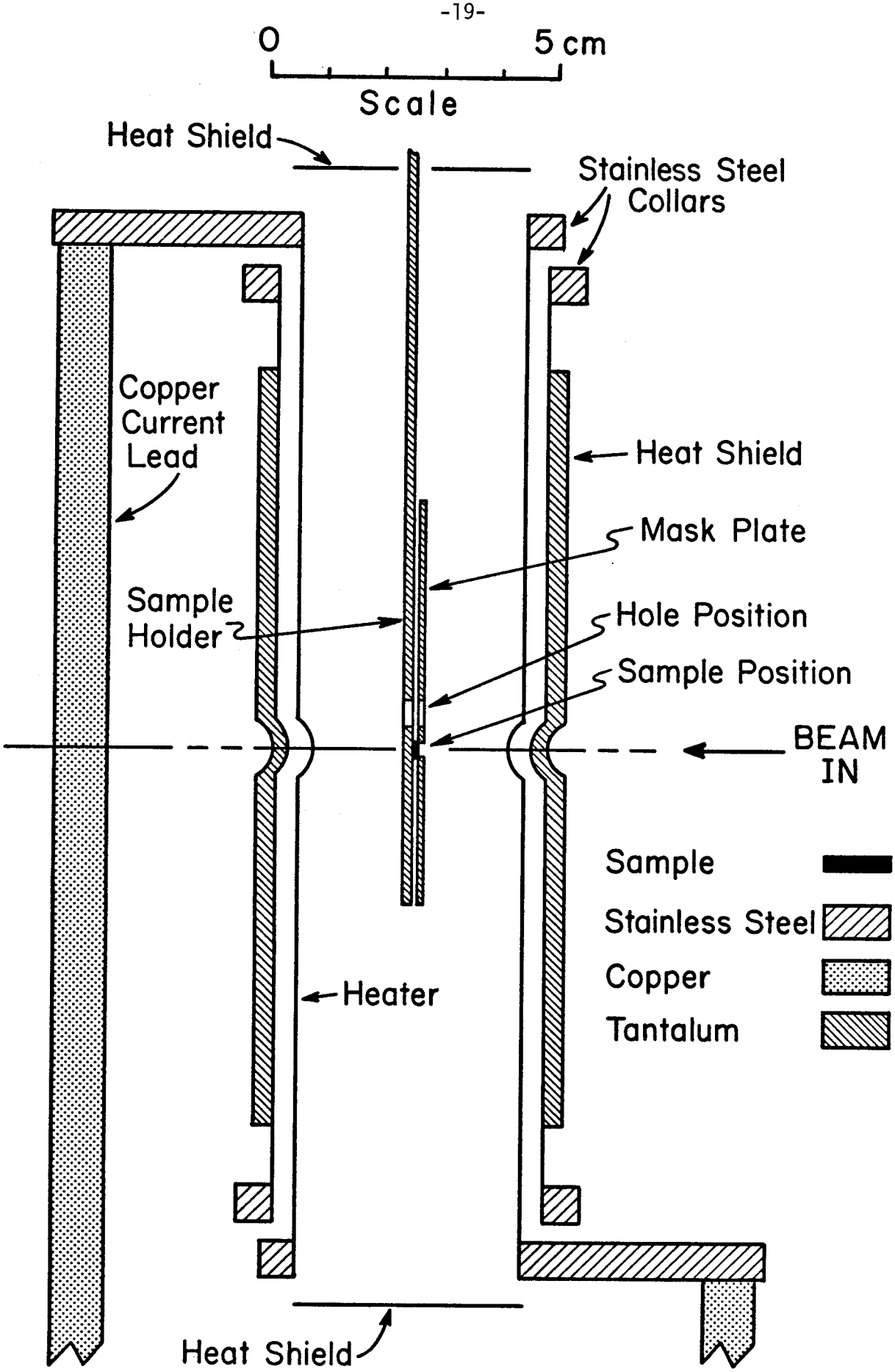
0
5 cm
Scale
Heat Shield
Stainless Steel
Collars
Copper
Current
Lead
Heat Shield
Mask Plate
Sample
Holder
Hole Position
Sample Position
BEAM
IN
Sample
Stainless Steel
Copper
Tantalum
Heater
Heat Shield

Figure 3

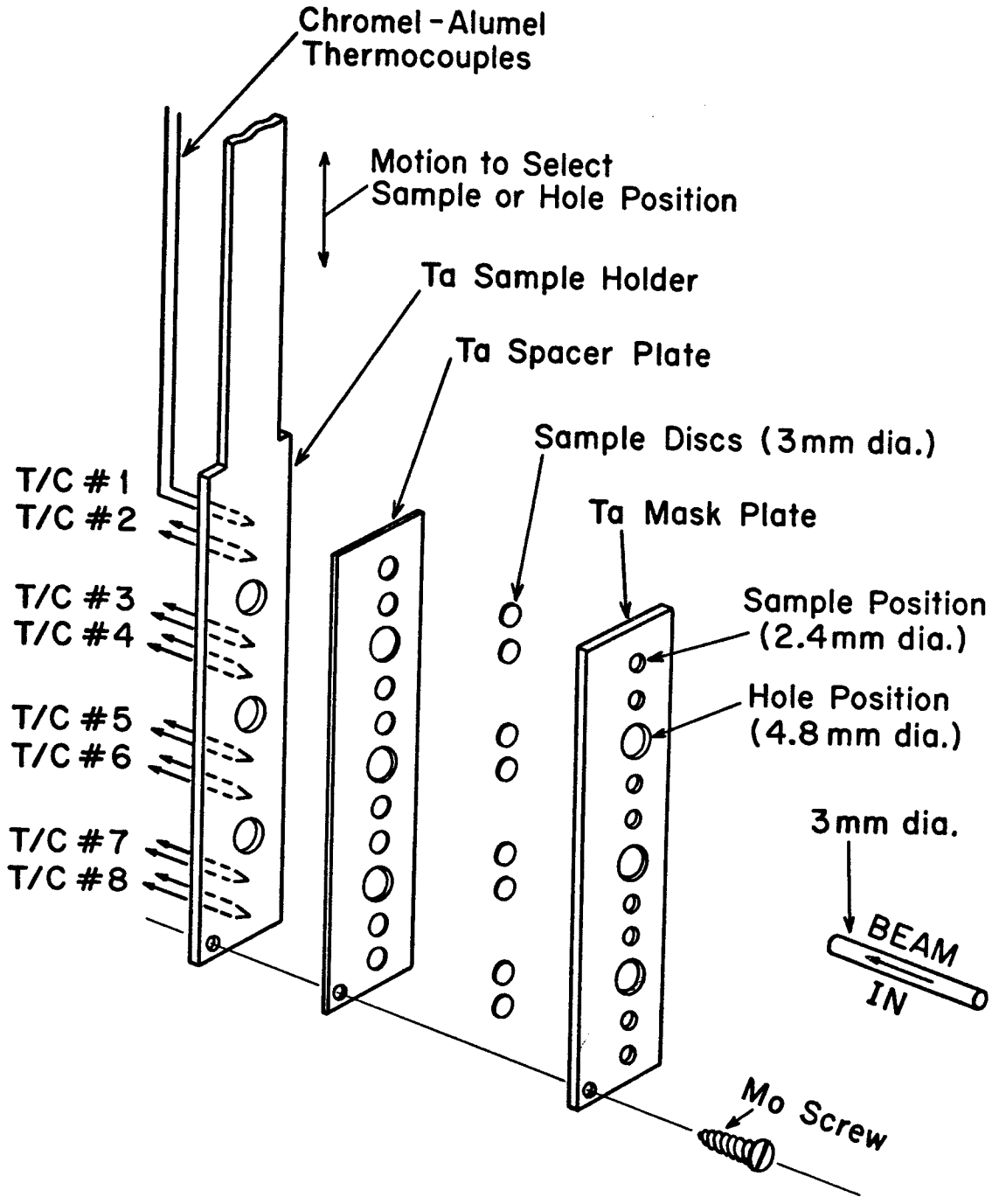


SAMPLE HOLDER (EXPLODED VIEW)

Figure 4

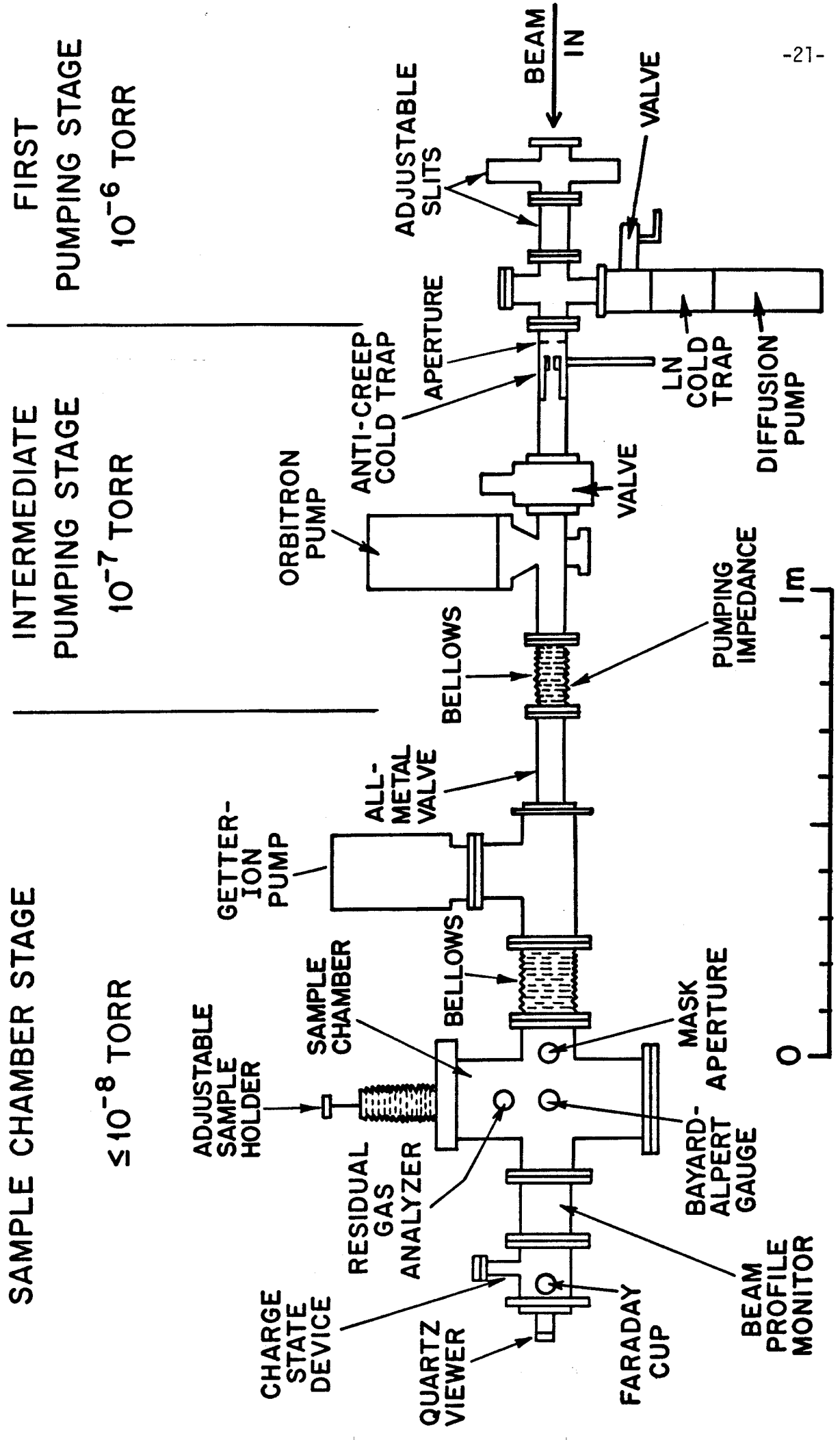
SAMPLE CHAMBER STAGE
≤ 10⁻⁸ TORR
INTERMEDIATE PUMPING STAGE
10⁻⁷ TORR
FIRST PUMPING STAGE
10⁻⁶ TORR
BEAM IN
ADJUSTABLE SLITS
VALVE
APERTURE
ANTI-CREEP COLD TRAP
LN COLD TRAP
DIFFUSION PUMP
ORBITRON PUMP
VALVE
BELLOWS
PUMPING IMPEDANCE
ALL-METAL VALVE
GETTER-ION PUMP
BELLOWS
SAMPLE CHAMBER
MASK APERTURE
ADJUSTABLE SAMPLE HOLDER
RESIDUAL GAS ANALYZER
BAYARD-ALPERT GAUGE
CHARGE STATE DEVICE
QUARTZ VIEWER
FARADAY CUP
BEAM PROFILE MONITOR
0
Scale
1m

Figure 5

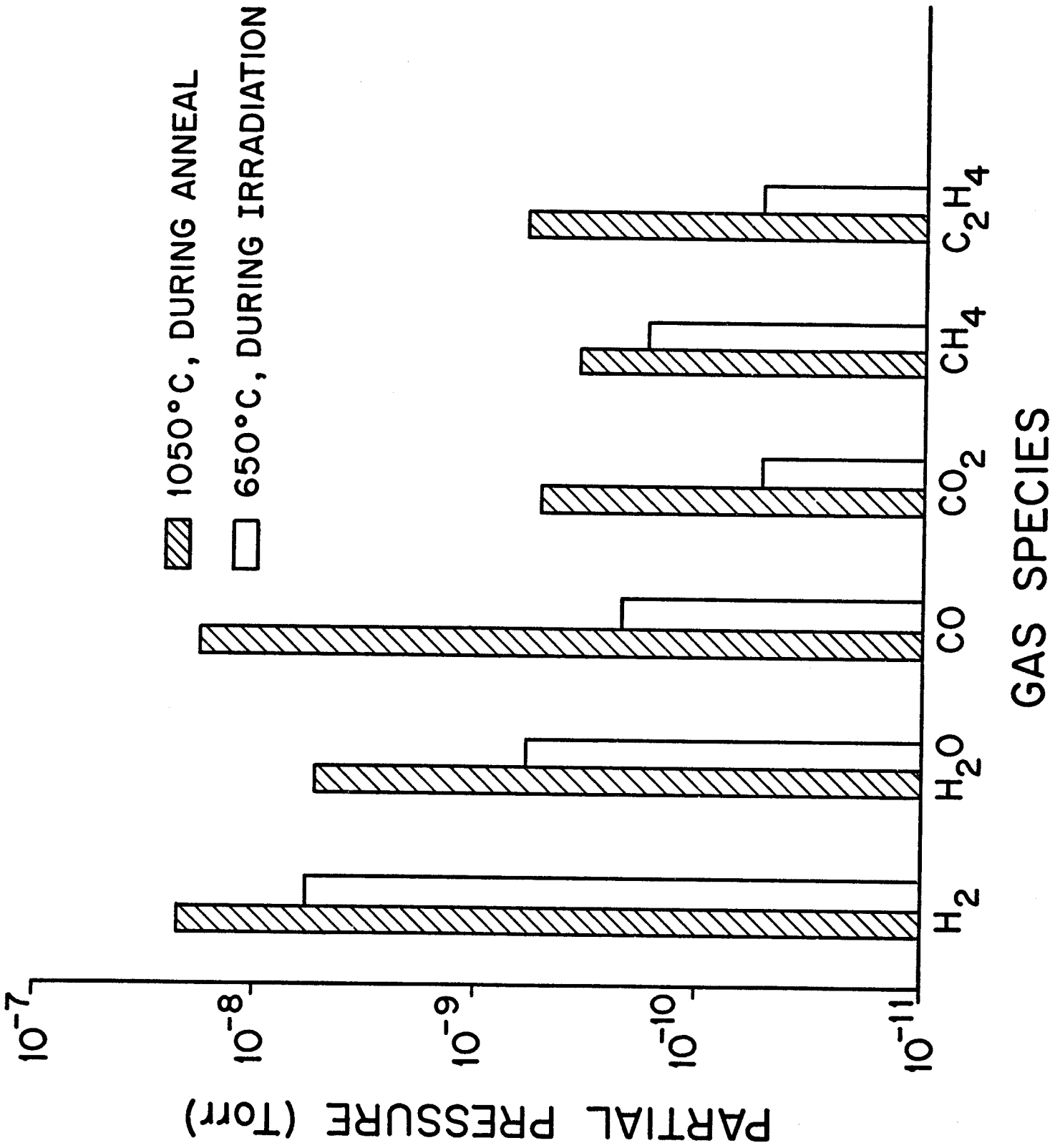
1050°C, DURING ANNEAL
650°C, DURING IRRADIATION
PARTIAL PRESSURE (Torr)
$10^{-7}$
$10^{-8}$
$10^{-9}$
$10^{-10}$
$10^{-11}$
$H_2$
$H_2O$
CO
$CO_2$
$CH_4$
$C_2H_4$
GAS SPECIES

Figure 6

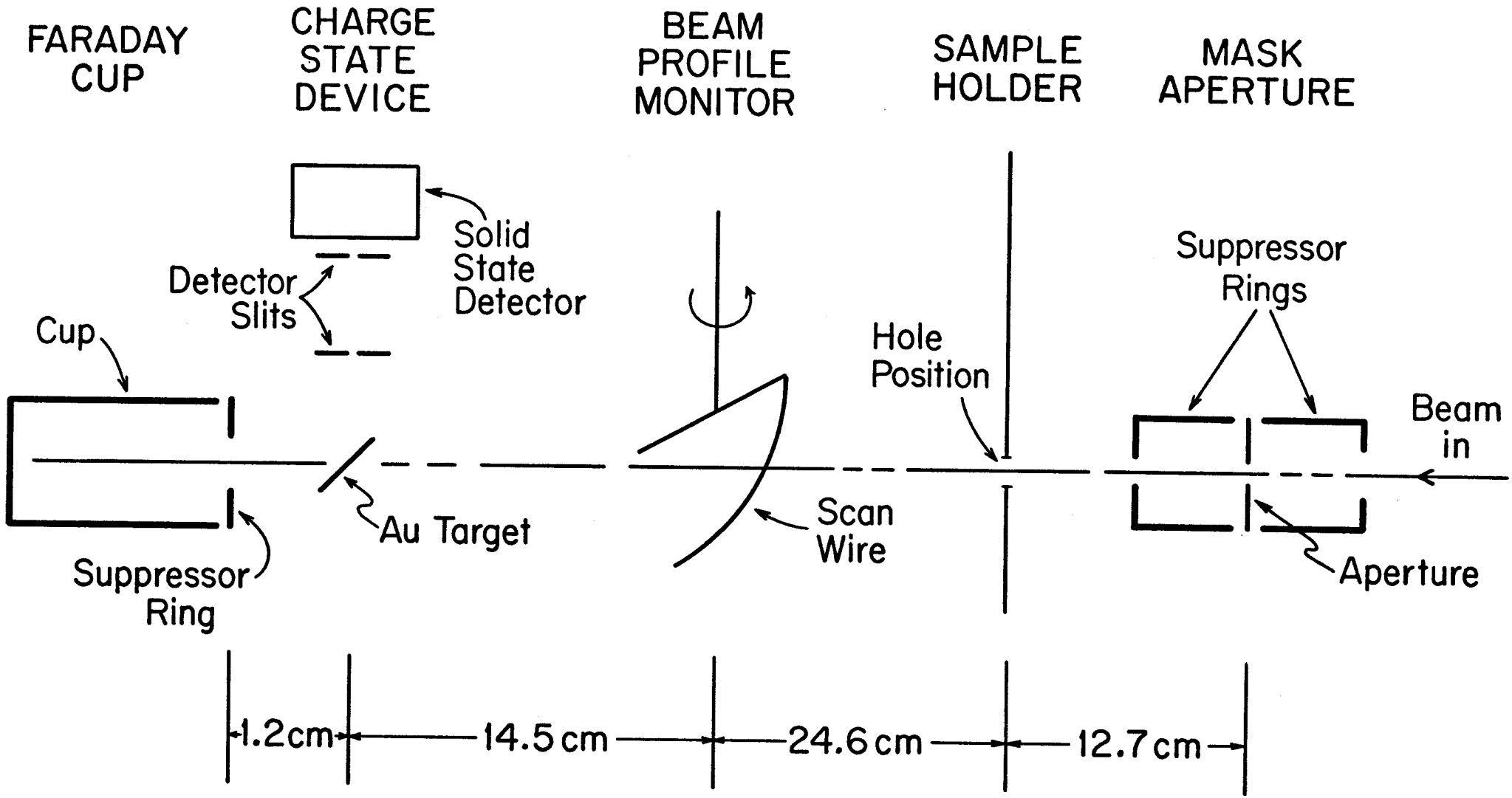
FARADAY CUP
CHARGE STATE DEVICE
BEAM PROFILE MONITOR
SAMPLE HOLDER
MASK APERTURE
Solid State Detector
Detector Slits
Cup
Suppressor Ring
Au Target
Scan Wire
Hole Position
Suppressor Rings
Beam in
Aperture
1.2cm
14.5 cm
24.6 cm
12.7 cm

Figure 7

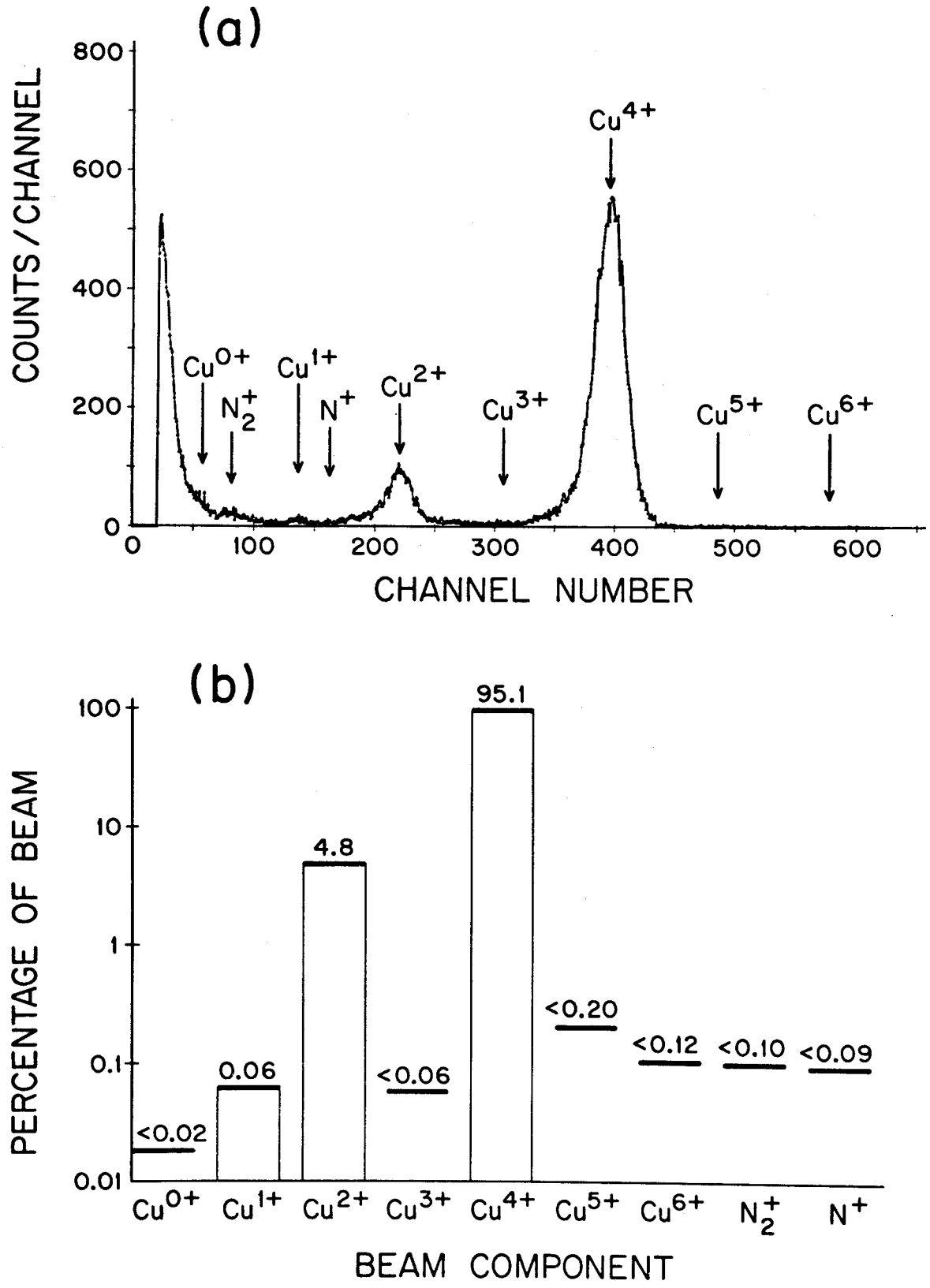
(a)
COUNTS/CHANNEL
800
600
400
200
0
0
100
200
300
400
500
600
CHANNEL NUMBER
Cu0+
N2+
Cu1+
N+
Cu2+
Cu3+
Cu4+
Cu5+
Cu6+
(b)
PERCENTAGE OF BEAM
100
10
1
0.1
0.01
95.1
4.8
<0.20
<0.12
<0.10
<0.09
0.06
<0.06
<0.02
Cu0+
Cu1+
Cu2+
Cu3+
Cu4+
Cu5+
Cu6+
N2+
N+
BEAM COMPONENT

Figure 8

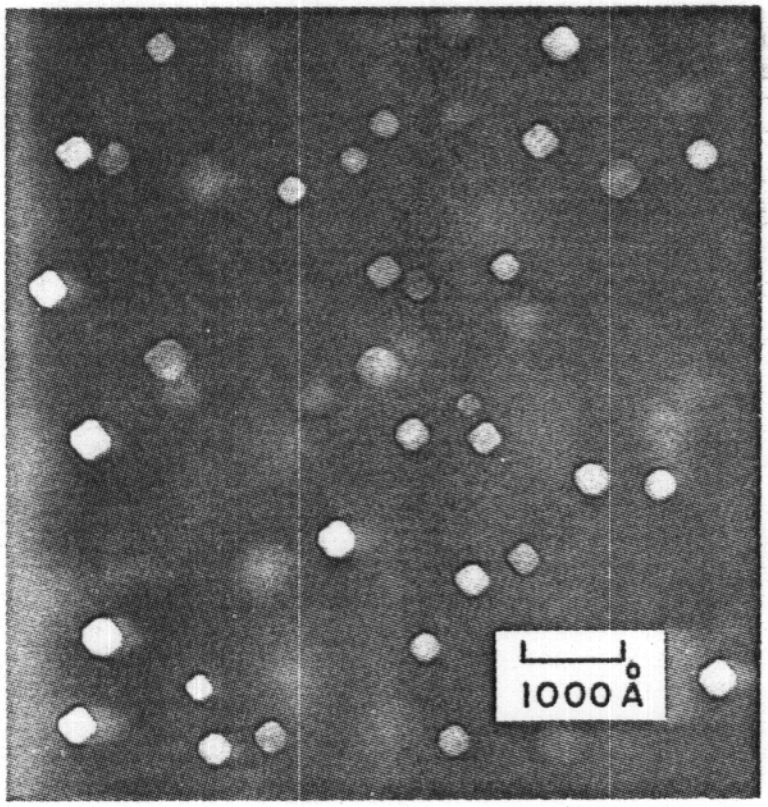


Figure 9